

# Characterization of the pressure fluctuations within a Controlled-Diffusion airfoil boundary layer at large Reynolds numbers

R. Boukharfane, J. Bodart, **M.C. Jacob**, L. Joly

ISAE-Supaero, Toulouse, France

T. Bridel-Bertomeu

French Alternative Energies and Atomic Energy Commission (CEA), Bordeaux, France

T. Nodé-Langlois

Acoustics Methods, Airbus Commercial Aircraft, Toulouse, France

# Outline

Introduction

Setting up three-dimensional simulations

Flow topology

Aerodynamics results

Frequency spectra of surface pressure fluctuations

Conclusions and Perspectives

## Airfoil Noise Mechanisms

Wall-pressure and loading fluctuations induced by a turbulent vortical field on a given airfoil can be caused by several mechanisms :

- Turbulence-interaction
- Noise Tip noise
- Vortex shedding noise
- Stall noise
- Trailing-edge noise

## Context

SCONE "Simulations of Contra Rotating Open Rotor (CrOr) and fan broadband NoisE with reduced order modelling"

- is part of the European CleanSky joint undertaking.
- aims at addressing the development of dedicated CROR/UHBR fan noise prediction tools.

## Objectives of the present study

- Carrying a large set of high fidelity simulations on simplified geometries (Controlled-Diffusion (CD) airfoil) relevant to CROR/UHBR fan trailing edge noise.
- Extract relevant quantities for TE noise modelling from large-eddy simulations.
- Comparison with experimental results.

### Controlled-Diffusion airfoil (rounded trailing edge)



Leading edge camber angle	Trailing edge camber angle	Thickness-to-chord ratio (max.)
12°	12°	4.5%

Table: Major geometrical characteristics of CD airfoil

## Motivation

- Accurate assessment of  $U_c$ ,  $\Phi_{pp}$  and  $\ell_z$  needs detailed spatial and temporal information regarding a wide range of turbulence scales.
- The capture of the **the spanwise correlation length  $\ell_z$**  can be ensured if and only if the span size of the computational domain  $L_z \geq 2\delta_{\max}$ , where  $\delta_{\max}$  is the maximum boundary layer thickness.

## Strategy for the simulation

- Estimate  $\delta_{\max}$  by performing a preliminary RANS simulation on a 2D mesh using Fluent (Boundary layer blocks refined to get  $y^+ \approx 1$  at the walls).
- Save computational time for the statistical convergence of the extruded 3D LES by performing a 2D simulation of the 2D mesh.
- Conduct the complete LES simulation on the extruded 2D mesh used in the second step.

Focus the numerical simulations on 7 specific operating points.

Configuration	$M_\infty$	$Re_c$	A.o.a	$\delta_{\max}$ (% c)	$L_z$ (% c)	$N_{\text{cells}}$
$C_1$	0.3	$8.30 \times 10^5$	$4^\circ$	3.4	10	225M
$C_2$	0.3	$8.30 \times 10^5$	$7^\circ$	7.1	20	451M
$C_3$	0.3	$2.40 \times 10^6$	$7^\circ$	7.3	20	451M
$C_4$	0.5	$2.29 \times 10^6$	$4^\circ$	3.3	10	225M
$C_5$	0.5	$2.29 \times 10^6$	$5^\circ$	4.8	20	451M
$C_6$	0.5	$2.29 \times 10^6$	$6^\circ$	6.1	20	451M
$C_7$	0.7	$2.40 \times 10^6$	$1^\circ$	5.3	20	451M

## Required amount of CPU time

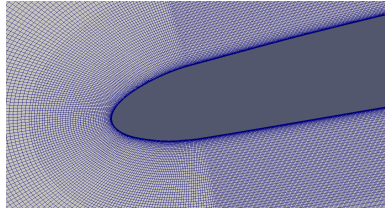
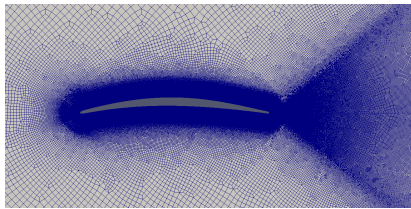
To conduct all these simulations, more than 11.5 million  $h_{\text{CPU}}$  have been used (CINES supercomputing center on Occigen and Barcelona supercomputing center on MareNostrum).

## Numerical solver : CharlesX

- High-fidelity unstructured compressible flow solver for LES (developed by CTR (Center for Turbulence Research) at Stanford University and ISAE/DAEP at Toulouse)
- It solves the spatially-filtered compressible N-S equations, using a finite volume formulation, control-volume based discretization on unstructured meshes.
- Background scheme is only non-dissipative for perfectly regular grids, but adds a small amount of numerical dissipation on irregular grids to aid the robustness.
- It benefits from the parallel performance: the code still fully exploit CPU based architectures with as low as 3000 grid points per CPU core

## Numerical details

- Extrusion in the spanwise direction with a uniform cell size over a length  $L_z$ .
- Vreman SGS model for the sub-grid terms.
- Unstructured control volume with a structured-like layer around the airfoil and unstructured elements in the far-field are used to reduce the computation cost.

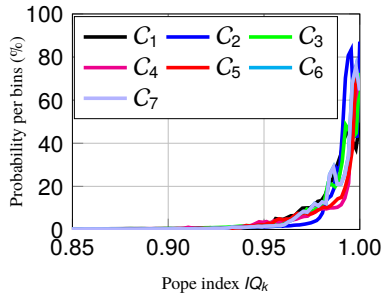


- Unsteady pressure signals are extracted from the computations using several probes located in the first wall-normal cell and goes all around the airfoil.

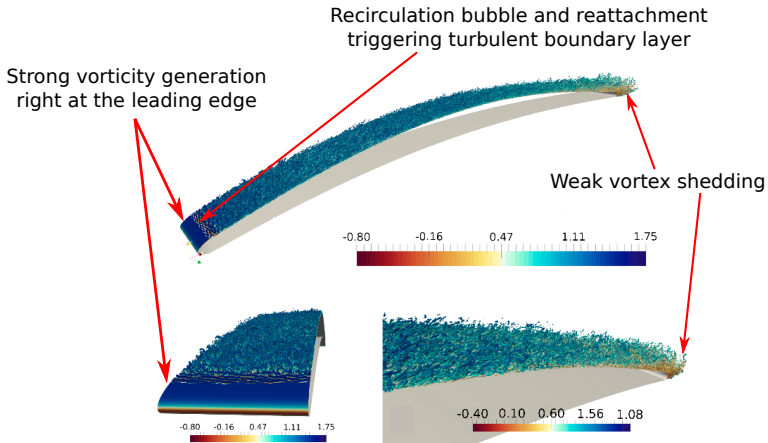
## Numerical verification

- Grid resolution along the blade surface
- Mesh resolution quality : Pope criterion  $IQ_k = \mathcal{K} / (\mathcal{K} + \mathcal{K}_{SGS})$ .

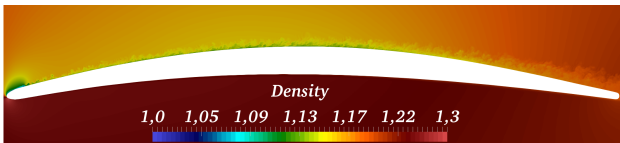
case	$\Delta x^+$	$\Delta y^+$	$\Delta z^+$
$C_1$	$\leq 28$	$\leq 1.02$	13.21
$C_2$	$\leq 27$	$\leq 1.04$	14.03
$C_3$	$\leq 29$	$\leq 1.11$	14.17
$C_4$	$\leq 28$	$\leq 1.12$	13.24
$C_5$	$\leq 26$	$\leq 1.22$	14.23
$C_6$	$\leq 24$	$\leq 1.20$	13.28
$C_7$	$\leq 23$	$\leq 1.09$	13.11



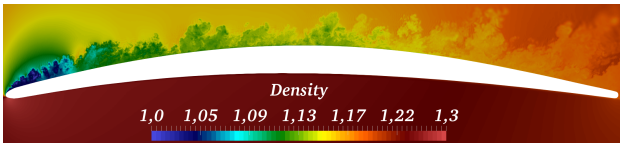
- ✓ Recommended orders of magnitude of computational mesh cell sizes ( $\Delta x^+ \sim 50 - 150$ ,  $\Delta y^+ < 2$  and  $\Delta z^+ \sim 10 - 40$ ) are quite satisfactorily met.
- ✓  $IQ_k \geq 0.94$ , the resolution level is excellent and almost reaches standard DNS resolution criteria (SGS model is almost inactive in the simulations)



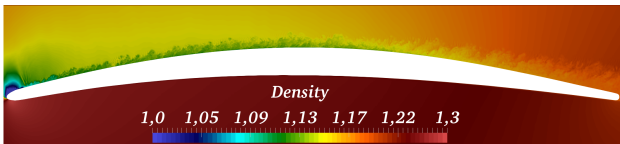
- ✓ A laminar boundary-layer is present on the lower side of the airfoil, and a transitional and turbulent boundary layer on the upper side.
- ✓ Detailed flow topology nicely captured for the case  $C_1$ .



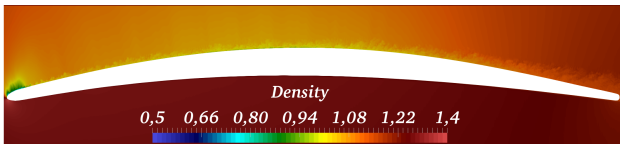
((1))  $C_1$  ( $M_\infty = 0.3$ ,  $Re = 8.30 \times 10^5$  et A.o.a=4°)



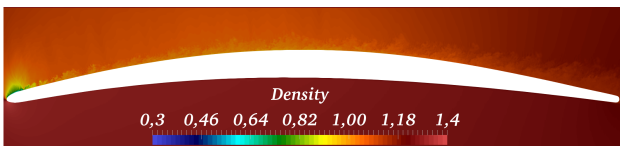
((2))  $C_2$  ( $M_\infty = 0.3$ ,  $Re = 8.30 \times 10^5$  et A.o.a=7°)



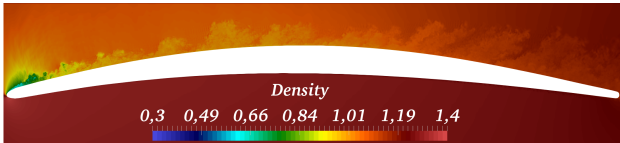
((3))  $C_3$  ( $M_\infty = 0.3$ ,  $Re = 2.40 \times 10^6$  et A.o.a=7°)



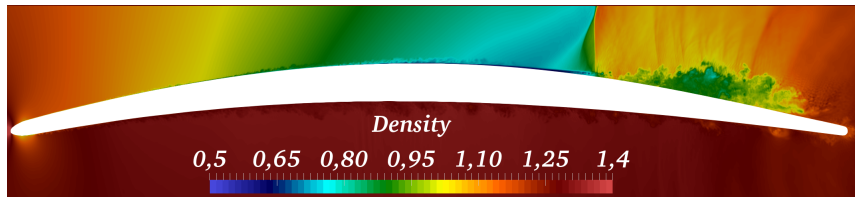
((4))  $C_4$  ( $M_\infty = 0.5$ ,  $Re = 2.29 \times 10^6$  et A.o.a=4°)



((5))  $C_5$  ( $M_\infty = 0.5$ ,  $Re = 2.29 \times 10^6$  et A.o.a=5°)



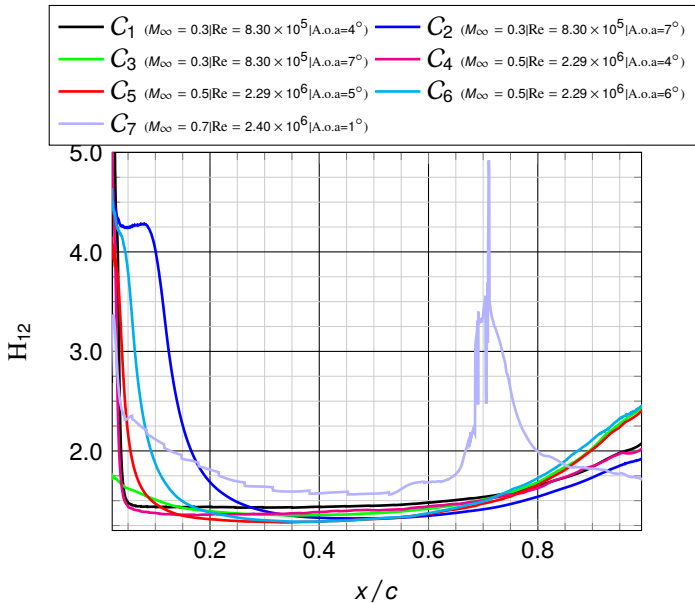
((6))  $C_6$  ( $M_\infty = 0.5$ ,  $Re = 2.29 \times 10^6$  et A.o.a=6°)



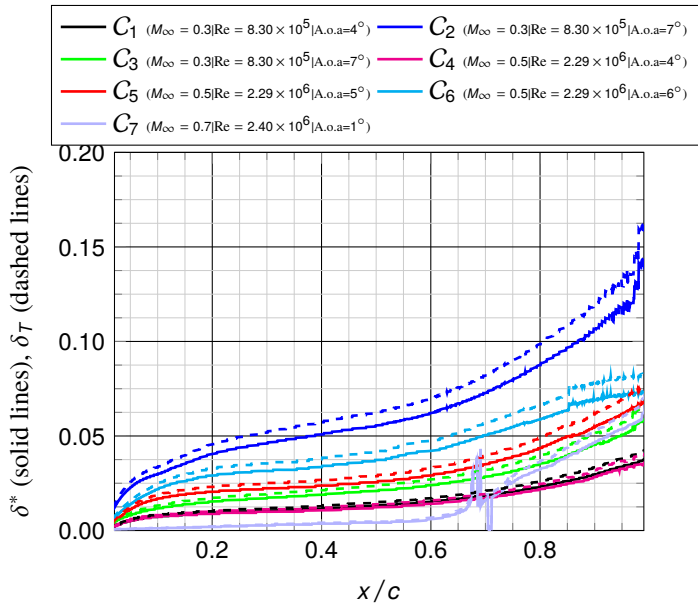
((7))  $C_7$  ( $M_\infty = 0.7$ ,  $Re = 2.40 \times 10^6$  et A.o.a=1°)

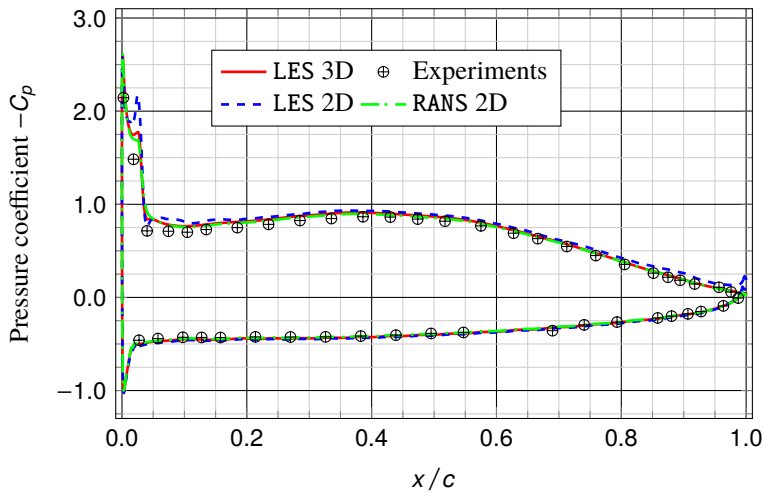
- Use of a shock sensor
- Formation of a weak shock on the suction side
- Stabilization of the shock stabilizes at around 65% chord.

└ Aerodynamics results

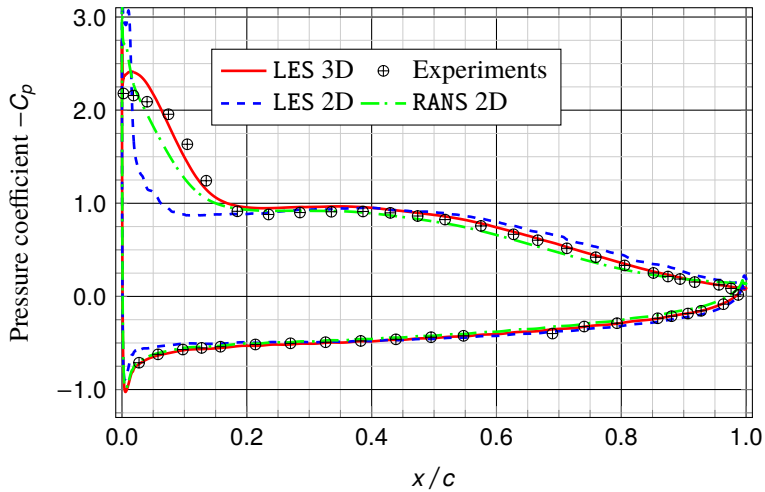
└ Shape factor  $H_{12} = \delta^* / \theta$ 

## └ Aerodynamics results

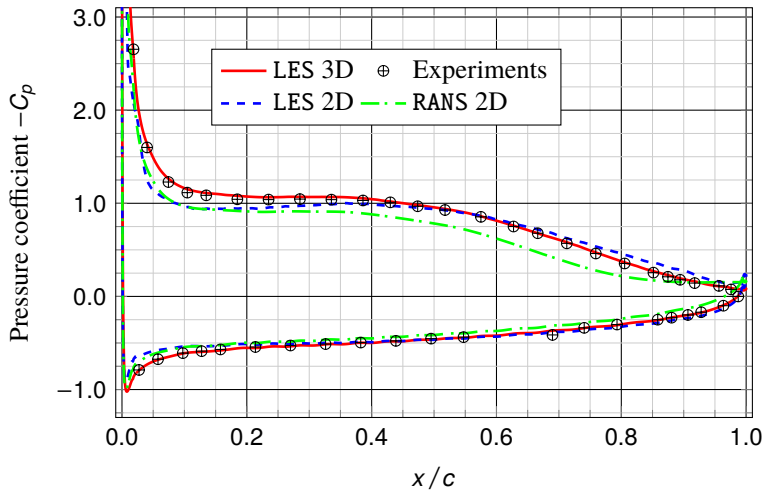
└ Displacement thickness  $\delta^*$  and thermal boundary layer thickness  $\delta_T$ 



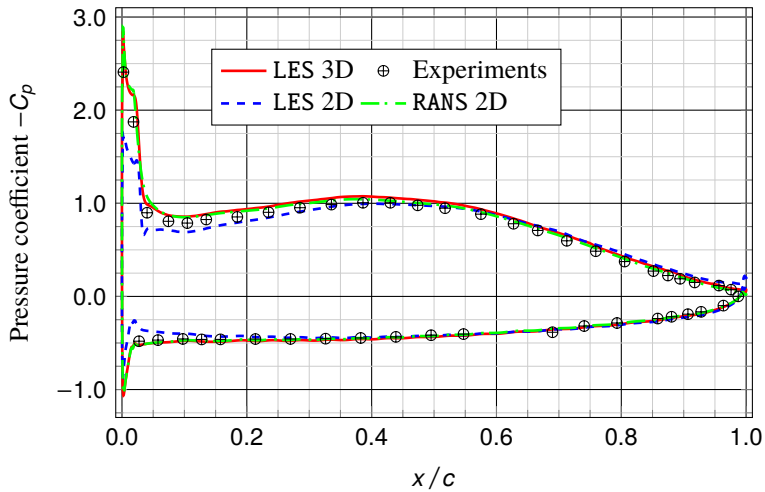
((8))  $C_1$  ( $M_\infty = 0.3$ ,  $Re = 8.30 \times 10^5$  et A.o.a=4°)



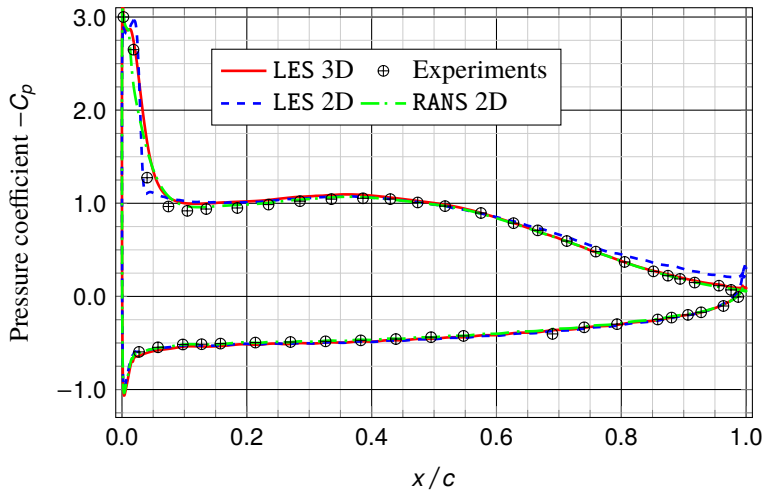
((9))  $C_1$  ( $M_\infty = 0.3$ ,  $Re = 8.30 \times 10^5$  et A.o.a=7°)



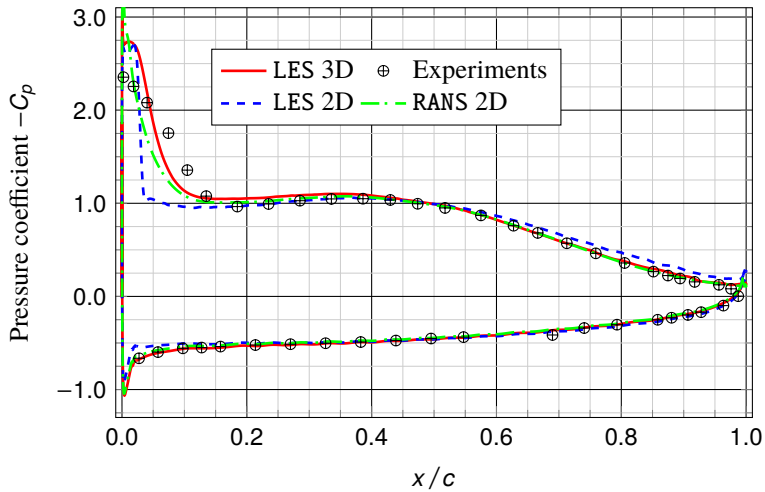
$$((10)) \quad C_1 \quad (M_\infty = 0.3, \text{Re} = 2.40 \times 10^6 \text{ et A.o.a}=7^\circ)$$



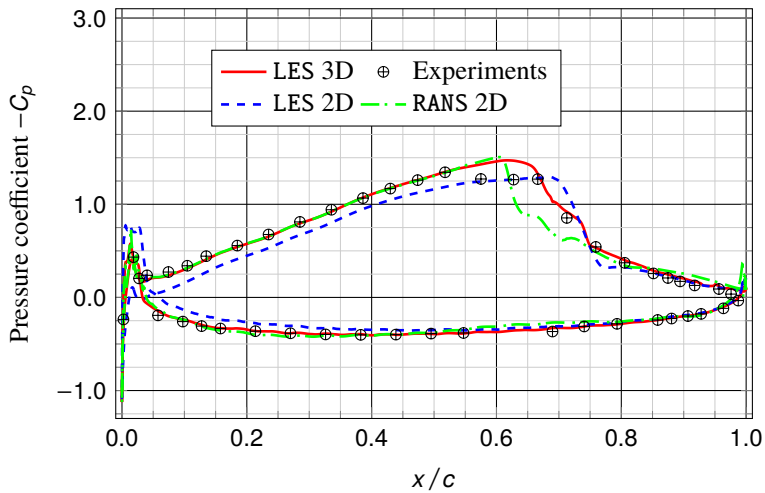
((11))  $C_4$  ( $M_\infty = 0.5$ ,  $Re = 2.29 \times 10^6$  et A.o.a=4°)



((12))  $C_5$  ( $M_\infty = 0.5$ ,  $Re = 2.29 \times 10^6$  et A.o.a=5°)



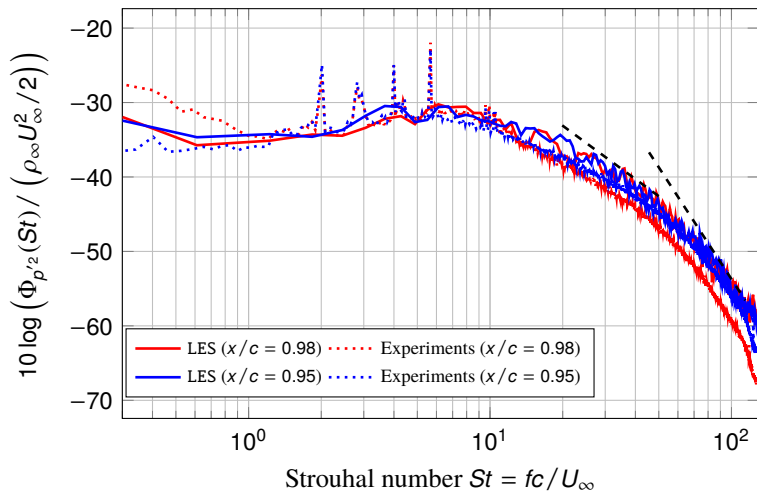
((13))  $C_6$  ( $M_\infty = 0.5$ ,  $Re = 2.29 \times 10^6$  et A.o.a=6°)



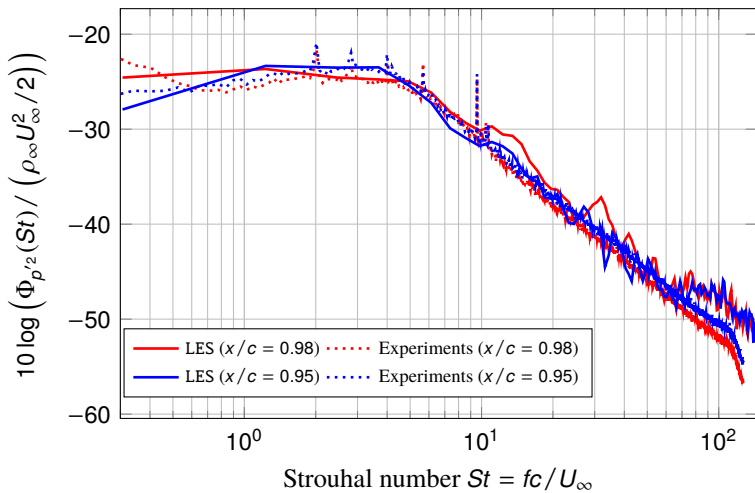
((14))  $C_7$  ( $M_\infty = 0.7$ ,  $Re = 2.40 \times 10^6$  et A.o.a=1°)

## Data acquisition

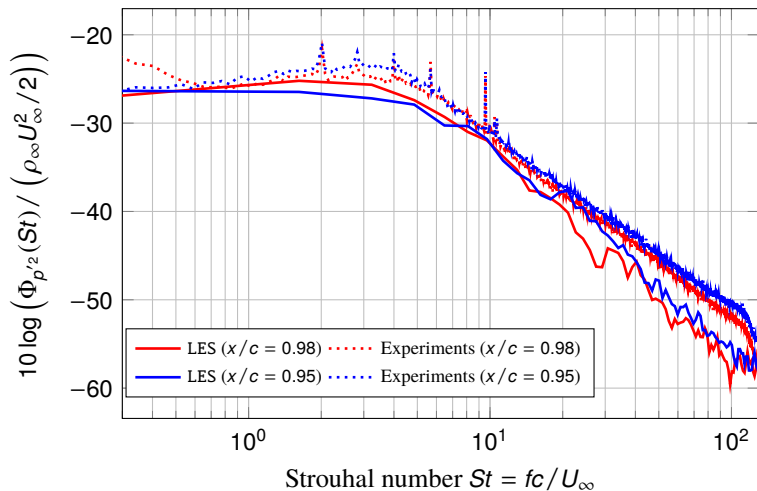
- Computations were run for 4 flow-through times before a statistically steady state was reached and mean values were collected.
- Airfoil surface pressure and velocity statistics were then acquired over a period of 18 (cases  $C_1-C_4$ ) or 15 (cases  $C_2-C_3-C_5-C_6-C_7$ ) flow-through times.
- Normalized sampling frequency of 600 (600 pressure and velocity samples are collected per probe and convective time scale  $t_c$ ).
- All spectral quantities are obtained using Welch's method considering segment of size  $N/16$ , where  $N$  is the number of sample of each case, with 50% overlap combined with the Hanning window function applied to each segments.



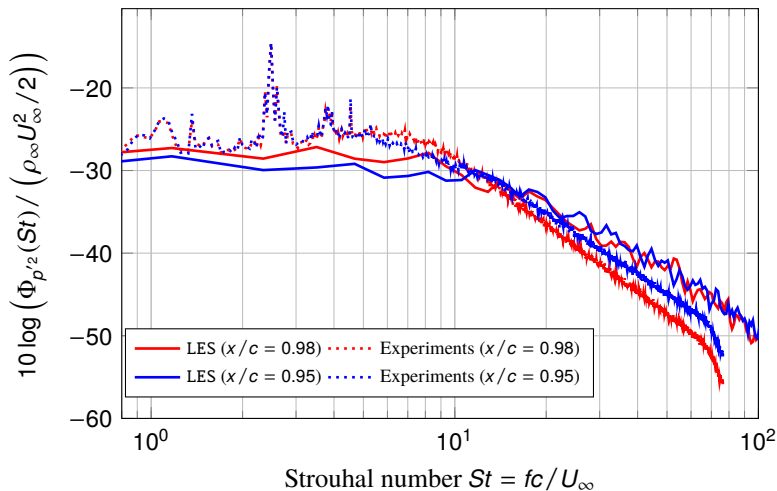
((15))  $C_1$  ( $M_\infty = 0.3$ ,  $Re = 8.30 \times 10^5$  et A.o.a=4°)



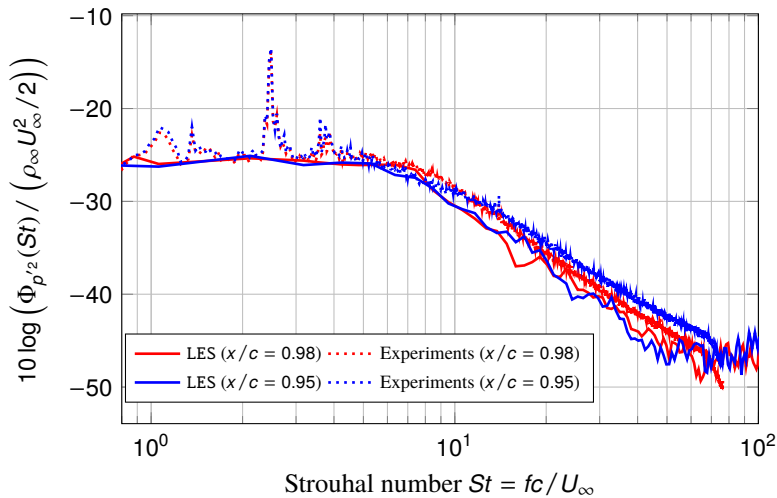
((16))  $C_2$  ( $M_\infty = 0.3$ ,  $Re = 8.30 \times 10^5$  et A.o.a=7°)



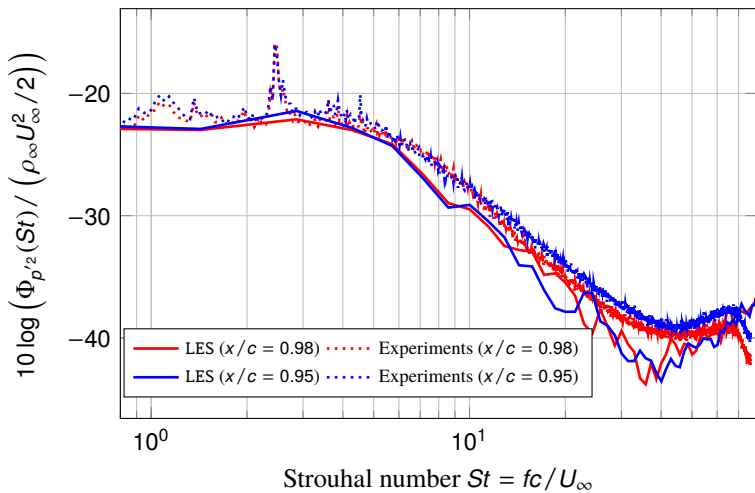
((17))  $C_3$  ( $M_\infty = 0.3$ ,  $Re = 2.40 \times 10^6$  et A.o.a=7°)



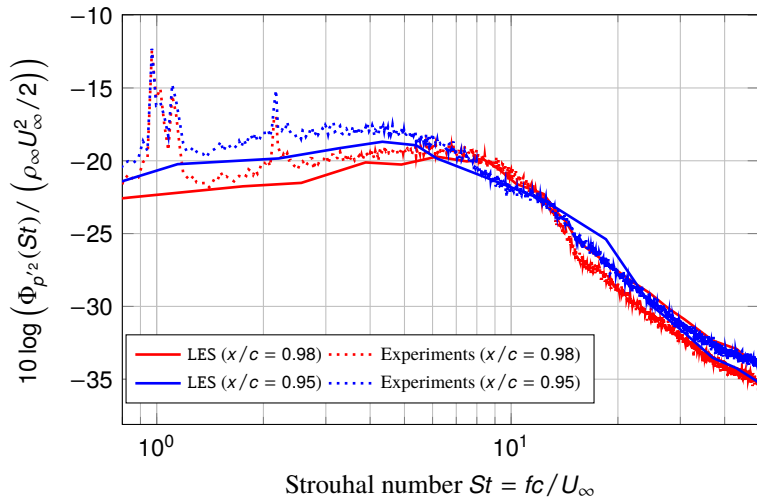
((18))  $C_4$  ( $M_\infty = 0.5$ ,  $Re = 2.29 \times 10^6$  et A.o.a=4°)



((19))  $C_4$  ( $M_\infty = 0.5$ ,  $Re = 2.29 \times 10^6$  et A.o.a=5°)



((20))  $C_6$  ( $M_\infty = 0.5$ ,  $Re = 2.29 \times 10^6$  et A.o.a=6°)



((21))  $C_7$  ( $M_\infty = 0.7$ ,  $Re = 2.40 \times 10^6$  et A.o.a=1°)

- └ Frequency spectra of surface pressure fluctuations
  - └ Spanwise coherence length

- The spanwise distribution is assumed to be homogeneous:

$$\ell_z(f) = \lim_{L \rightarrow \infty} \int_0^L \sqrt{\gamma^2(\Delta z, f)} d(\Delta z)$$

- Based on Corcos work for the spanwise coherence length of a flat plat turbulent boundary layer at equilibrium

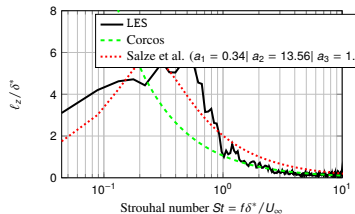
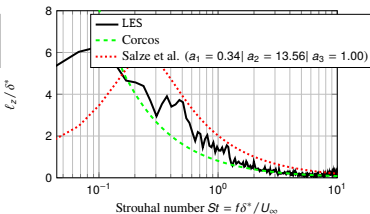
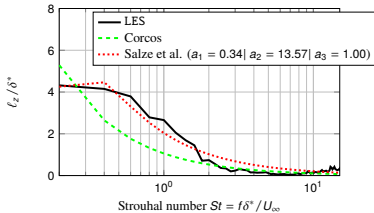
$$\ell_z \approx b U_c / f$$

- Salze model based on Efimtsov theory

$$\ell_z = \delta^* \left[ \left( \frac{a_1 f \delta^* U_\infty}{c U_c} \right)^2 + \frac{a_2^2}{f \delta^* (H_{12}^2 U_\infty / u_\tau)^2 / c + (a_2/a_3)^2} \right]^{-1/2}$$

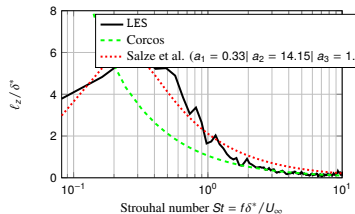
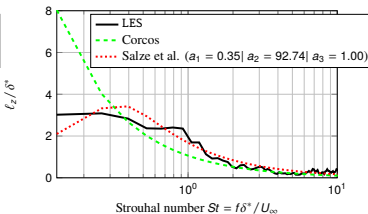
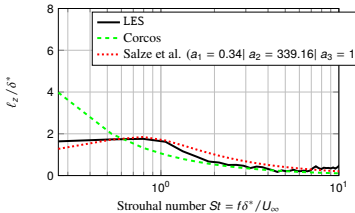
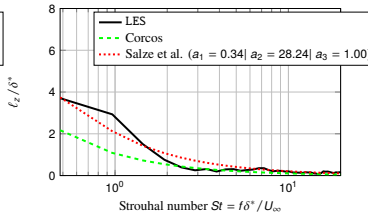
└ Frequency spectra of surface pressure fluctuations

└ Spanwise coherence length

((22))  $C_1$ ((23))  $C_2$ ((24))  $C_3$

└ Frequency spectra of surface pressure fluctuations

└ Spanwise coherence length

((25))  $C_4$ ((26))  $C_5$ ((27))  $C_6$ ((28))  $C_7$

## Conclusions

- Very good matching with experiments despite:
  - ✓ different inflow conditions (At LE, the flow is fully laminar in the simulations)
  - ✓ Wind tunnel BPF in experiments
- confidence in the predictions in the region of interest (TE)
- On-going analysis of the relevant quantities
- “Large” physical time required to reach convergence in the high order statistics
- Identifications of the scaling quantities

## Perspectives

- Validation of the wall modelling approach on non rotating cases
- Sliding mesh computations of a single rotating blade using wall-modelling.